

# Separation of Insect Trajectories in Dynamic Vision Sensor Data

Juliane Arning<sup>1</sup> and Christoph Dalitz<sup>1</sup><sup>a</sup> and Regina Pohle-Fröhlich<sup>b</sup>

<sup>1</sup>*Institute for Pattern Recognition, Niederrhein University of Applied Sciences, Reinarzstr. 49, Krefeld, Germany*  
christoph.dalitz@hsnr.de

Keywords: Event Camera, Clustering, Insect Monitoring.

Abstract: We present a method to separate insect flight trajectories in dynamic vision sensor data and for their mathematical description by smooth curves. The method consists of four steps: Pre-processing, clustering, post-processing, and curve fitting. As the time and space coordinates use different scales, we have rescaled the dimensions with data-based scale factors. For clustering, we have compared DBSCAN and MST-based clustering, and both suffered from undersegmentation. A suitable post-processing was introduced to fix this. Curve fitting was done with a non-parametric LOWESS smoother. The runtime of our method is sufficiently fast to be applied in real-time insect monitoring. The data used for evaluation only had two spatial dimensions, but the method can be applied to data with three spatial dimensions, too.

## 1 INTRODUCTION

The “Krefeld Study” from 1989 to 2016 (Hallmann et al., 2017) has shown a decline in flying insect biomass of more than 75 percent, which has raised considerable interest in insect monitoring. The Krefeld Study utilised Malaise traps. These kill the trapped insects, which are subsequently manually classified and weighted in a tedious process, and it would be desirable to have another method available that is nonlethal and less time consuming.


The BeeVision project (Pohle-Fröhlich and Bolten, 2023) addresses this problem and explores the use of Dynamic Vision Sensors (DVS) for monitoring flying insects. These sensors detect local variations in brightness and trigger events only for brightness variations greater than some threshold. Position, time, and the sign of the brightness change are recorded for each event. Unlike traditional frame based cameras, DVS operate almost continuously and do not yield frames, but point clouds. This has the advantage of a much higher time resolution and a smaller data size, but it requires special algorithms for identifying and separating insect tracks in point clouds.


Insect tracks occur in DVS point clouds as piecewise continuous dense strips. These can be interrupted by gaps due to occlusion by other objects. Moreover, rest periods on, e.g., flowers lead to in-

terruptions, too, because dynamic vision sensors only see moving objects. Starts and landings on plants can also lead to sharp turns in the flight path, so that the flight trajectories are not necessarily smooth.

The problem thus consists in partitioning a point cloud into an unknown number of clusters representing insect tracks and another cluster representing noise. This is similar to the problem of particle track identification in Time Projection Chambers (Dalitz et al., 2019a). Although there are algorithms like CLUE (Rovere et al., 2020) or TriplClust (Dalitz et al., 2019b) that have been devised for this particular use case, we have not been successful in applying them to our data. CLUE requires an energy for each event, which was lacking in our data and therefore had to be replaced by some dummy value, and we found no parameter settings for the implementation CLUEstering<sup>1</sup> that worked in our use case. The use of TriplClust was not feasible due to its high time and space complexity: For instance, a noise free DVS recording of approximately 160 seconds required about 126 GB of memory in TriplClust.

We therefore resorted to density based clustering methods like DBSCAN (Ester et al., 1996) and MST splitting (Zahn, 1971). These showed deficiencies in our use case, too, especially in challenging scenarios, such as when insect tracks cross each other. In the present report, we discuss how these shortcomings can be overcome, with special attention on improving the runtime in order to enable processing in real-time.

<sup>a</sup> <https://orcid.org/0000-0002-7004-5584>

<sup>b</sup> <https://orcid.org/0000-0002-4655-6851>

<sup>1</sup><https://github.com/cms-patatrack/CLUEstering>

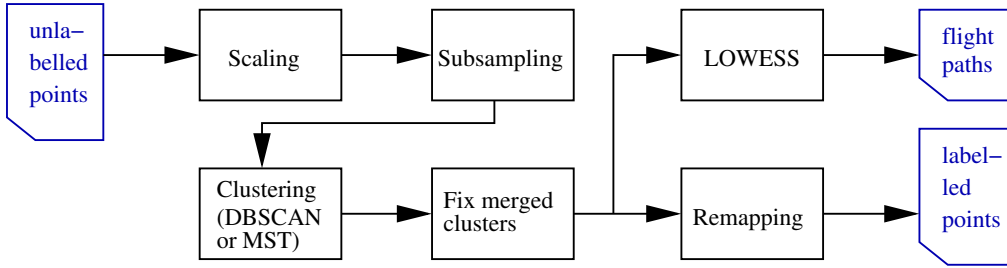


Figure 1: Processing pipeline of the segmentation method.

To this end, we utilised octree subsampling and time rescaling, modifications to the clustering algorithms, and a special post-processing for dealing with under-segmentation that is inherent to the clustering algorithms. After mapping the subsampled clusters back to the original data, the flight trajectories can be interpolated with a LOWESS (Cleveland, 1979) multivariate regression based on the time as a single predictor. All of these methods are described in section 2.

We evaluated our method on a series of DVS recordings provided by the BeeVision project, where insect events had already been segmented from other events with a lightweight U-Net (Pohle-Fröhlich et al., 2024). This enabled us to evaluate the algorithm both with and without the presence of background noise stemming from shaking leaves, varying illumination due to clouds, or other random effects. The evaluation is described in section 3.

## 2 SEGMENTATION METHOD

The segmentation algorithm takes an unlabelled point cloud with time and space coordinates as input and returns two output lists: For each point, a cluster label or a noise label is computed, and for every non-noise cluster a fitted flight path is computed and sampled at equidistant timestamps. The processing pipeline of the algorithm is shown in Figure 1. It consists of the following steps: Pre-processing, clustering, post-processing, fitting of flight paths using the LOWESS method, and remapping the labels to the original point cloud. Additionally, after reading of the input CSV-file, the timestamp is scaled by a scaling factor that was determined for representative data.

During pre-processing, the data is subsampled and outliers are removed. This smaller point cloud is then clustered. The clustering has a tendency to undersegment nearby insect tracks. These tracks are therefore corrected in the post-processing step. Afterwards, curves representing flight paths are fitted and the spatial curve position is computed for equidistant timestamps. Since the clustering was done on only the

subsampling and filtered data, labels must be propagated to the points that were removed during pre-processing. To this end, every unlabelled point receives the label of the nearest labelled point. The individual steps are described in detail in the following subsections.

### 2.1 Pre-processing

The timestamp dimension  $t$  is of a different unit (microseconds) and thus differs several orders of magnitude from the spatial dimensions (pixel). With the original timescale of microseconds, the distances in the temporal dimension thus dominate the distances of the spatial dimensions, which has a serious negative impact on the performance of DBSCAN and the MST-based clustering methods.

We therefore scale the time with a data based scaling factor. As the DVS recording scenario is the same for all recorded data, it was sufficient to estimate an appropriate scaling factor only once from a representative subset of the data. We have chosen the scaling factor  $s$  such that the mean distances to the  $k$ -th nearest neighbour in the spatial direction  $\bar{d}_x(k)$  and  $\bar{d}_y(k)$  is equal to the mean distance  $\bar{d}_t(k)$  in the  $t$  direction, i.e.

$$s \cdot \bar{d}_t(k) = (\bar{d}_x(k) + \bar{d}_y(k)) / 2 \quad (1)$$

It is interesting to note that the scale factor  $s$  was quite

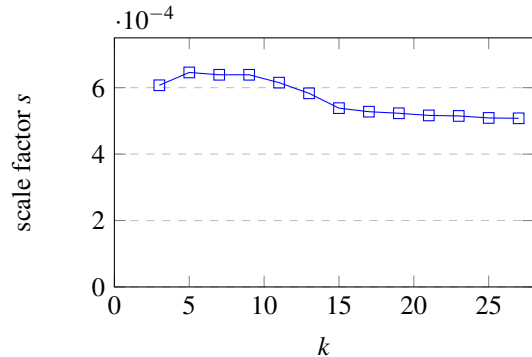


Figure 2: Dependency of the scaling factor  $s$  according to Eq. (1) on the number of neighbours  $k$ .

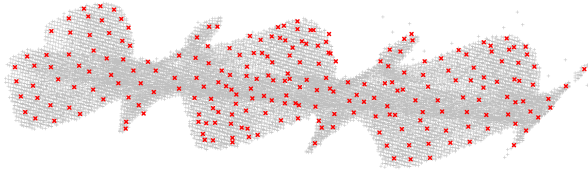


Figure 3: Subsampling: grey points are the original point cloud and the red crosses are the subsampled points

robust with respect to the choice of  $k$ , as can be seen in Figure 2. Moreover, we have observed that either choice in this range resulted in a similar performance of the clustering algorithm, and we have settled on  $s = 5.3 \cdot 10^{-4} \mu s^{-1}$ .

After scaling the timestamps, an octree-based subsampling is applied in order to reduce both data volume and noise. Octree subsampling works by constructing a tree structure that recursively divides the 3D space into eight evenly-sized cubes, stopping at a predefined depth (Meagher, 1982). This process leaves the non-empty space divided into cubes, and for each cube a representative point is selected. These representative points form the subsampled point cloud. To make the filtering effect independent from the size of the point cloud, we chose the side length of the cube at the lowest level of the octree as the stopping criterion instead of the depth. A larger value causes more filtering and a smaller value less filtering. In our use case, the full octree data structure was not needed, because no nearest-neighbour queries are done on the full point cloud, only on the subsampled data. We therefore divide the space directly into cubes.

There are different options to select the representative point, e.g., the point closest to the centroid of the cube, or the point closest to the centroid of the points in the cube. This, however, has only little effect on the results. A result of the subsampling step is shown in Figure 3. The octree subsampling has the positive side-effect that it can also be used for removing noise in sparse regions simply by skipping cubes with fewer points than a defined threshold. This simple noise reduction step does not increase the runtime; it only requires some additional space since the skipped points have to be memorised in order to obtain the noise label in the remapping step.

## 2.2 Clustering

As neither the number of insect tracks, nor their shape is known, we cannot use clustering algorithms like k-means that look for spherical clusters and a given number of clusters. A characteristic of insect flight trajectories is that they typically are represented by re-

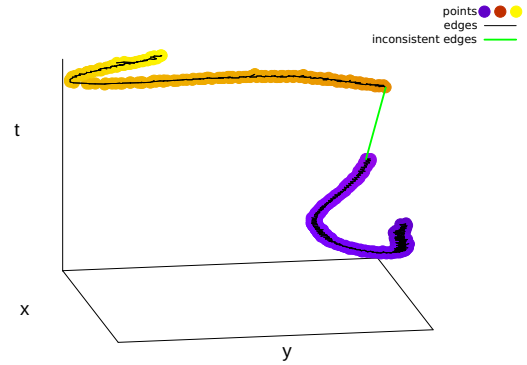


Figure 4: The MST of two clusters with an “inconsistent edge” highlighted in green and the points coloured by cluster.

gions with a higher point density and are separated by less dense regions. It is thus natural to use a clustering method based on closeness of points and thus a local density. We have implemented both DBSCAN and MST-based clustering as alternative options. Both are clustering algorithms that can detect clusters of arbitrary shape and do not require the number of clusters beforehand.

MST-based clustering algorithms build a weighted graph with weights corresponding to the Euclidean distance between node points, and remove “inconsistent edges” from the Minimum Spanning Tree (MST) of this graph (Zahn, 1971). Edges are considered “inconsistent” if they have a weight that is above some global or local distance threshold. This splits the MST into connected components which represent the clusters. The MST-based clustering method is illustrated in Figure 4 with the MST of two insect tracks. The inconsistent edge highlighted in green is removed, which results in two connected components representing insect tracks. These can be easily identified using graph traversal techniques such as breadth-first or depth-first search.

In general, building an MST for  $N$  nodes has runtime complexity  $O(N^2)$ , but as our distance is Euclidean, it is not necessary to build the complete distance matrix and the runtime can be reduced to  $O(N \log N)$  (March et al., 2010). Moreover, we could rely on a fast Open Source C++ implementation by Andrii Borziak<sup>2</sup>.

Due to a considerable spread in point density between different tracks, local thresholds for identifying inconsistent edges resulted in undersegmentation. We therefore used a global threshold for removing incon-

<sup>2</sup><https://github.com/AndrewB330/EuclideanMST>

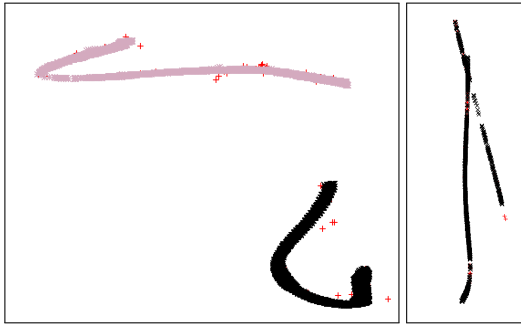


Figure 5: MST-based segmentation works in the example on the left, and fails in the example on the right. The same occurs for DBSCAN.

sistent edges, which was chosen in dependence of the length  $d$  of the pre-processing octree cube diagonal as  $5 \cdot d$ . However this threshold is chosen, there are two unavoidable problems: Splits due to gaps in partially occluded tracks, and merges of tracks coming close to each other. An example can be seen in Figure 5.

The MST-based clustering also offers a simple method identify falsely recognised clusters in dense regions that actually represent noise. When the edges are traversed in the MST, the mean edge weight can be calculated. Clusters with a small mean edge weight can be removed as they often consist of noise. This method adds more robustness against very strong noise, which is common in DVS-recordings and cannot be removed by the filtering in the subsampling step.

DBSCAN (Ester et al., 1996) is a density-based clustering algorithm, that defines clusters as regions of high density that are separated by regions of lower density. DBSCAN has two parameters,  $eps$  and  $minPts$ . Every point with at least  $minPts$  neighbours within a radius of  $eps$  is a core point. Whenever an unlabelled core point is found, a new cluster is initialised and the core point is added to it. The new cluster is iteratively propagated to core points within radius  $eps$ . This process is iterated until all core points and their neighbours are assigned to clusters. Points that are not neighbours of a core point are marked as outliers.

Schubert et al. (Schubert et al., 2017) suggested simple heuristics for choosing the parameters. For  $minPts$ , they suggested  $minPts = 2 \cdot \#Dimensions = 6$ , which we have adopted. We have not utilised their suggestion to analyse a 'k-dist plot' to determine an appropriate  $eps$ , because the octree cell size of our subsampling process already limits the possible maximum point density. We therefore set  $eps$  equal to a multiple of the diagonal of the cube, which is the furthest distance between two points in a dense insect track should be separated. After experimentally test-



Figure 6: Example for two merged tracks that are correctly split up during post-processing.

ing different values for the multiplication factor, we settled on  $eps = 6 \cdot d$ , where  $d$  is the diagonal length of a cell in the pre-processing octree.

Like MST-based clustering, DBSCAN cannot separate tracks when insect tracks come close to each other (see Figure 5), because both algorithms are purely based on point distances. To correct this problem, a post-processing step is necessary.

## 2.3 Post-Processing

To separate touching insect tracks that were erroneously merged into the same cluster, we implemented a post-processing that consists of three steps. First, possibly merged clusters are identified and, secondly, these clusters are split up at branching points in their Minimum Spanning Tree (MST). As the splitting leads to oversegmentation, that is corrected in the third step by merging the most appropriate branches based on their direction and time alignment. An example can be seen in Figure 6.

### 2.3.1 Identifying Merged Clusters

To minimise runtime and prevent over-segmentation, we first detect merged clusters using a simple heuristic. This approach is based on the premise that when insect tracks intersect, there should be simultaneous activity in different spatial regions at the same time. As an indicator for this phenomenon, we compute the spatial Euclidean distance between consecutive time points for each cluster, which results in an array of  $n - 1$ -values which we call  $\Delta s$ . The computation is facilitated by the nature of the DVS stream, which

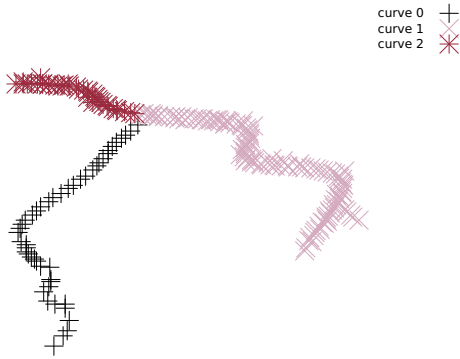


Figure 7: Example for oversegmentation due to splitting at crossing points

records events according to their time order, so that consecutive points occur at similar times.

If the standard deviation of the array  $sd(\Delta s)$  exceeds a threshold  $\theta_{sd}$ , the cluster is flagged for further post-processing steps. In the longest recording and for the threshold value  $\theta_{sd} = 22.36$  that worked best in our case, 16 out of 598 clusters met this criterion, including all 12 merged tracks and 4 incorrect classifications.

### 2.3.2 Splitting Clusters

For each flagged cluster, an MST is built and nodes with three or more branches of sufficient depth are identified as split points. The depth threshold is chosen proportional ( $\alpha \cdot n_i$ ) in order to adapt it to varying cluster sizes. At each split point, all edges except the shortest one are deleted. This splits the cluster into connected components, which are identified and numbered. These preliminary clusters are referred to as segments. These must be further processed, though, because the splitting method can result in oversegmentation at X-crossing points where the straight continuation cannot be preserved (see Figure 7).

### 2.3.3 Merging Over-Segmented Components

To correct over-segmentation due to MST splitting, segments are merged again, if they are continuations of each other in the direction extrapolated from the end of the earlier segment. For every segment  $S_i$  that occurred during splitting the clusters at branches, another fitting segment  $S_j$  is sought as continuation. Both the time order of both segments is considered, as well as the direction of the segments around the ends with the closest timestamps.

Only segments  $S_j$  with timestamps greater than  $S_i$ , within a given tolerance and with a sufficiently small gap, are considered. The time difference between the last point of  $S_i$  ( $t_e$ ) and the first point of  $S_j$  ( $t_s$ ) must

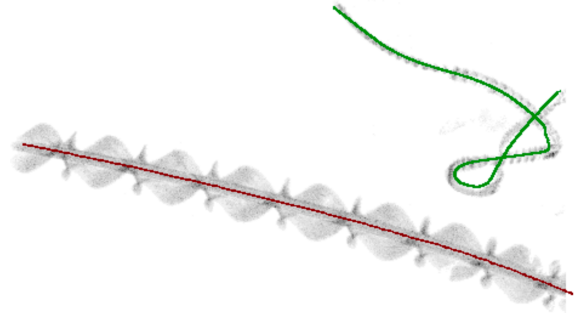


Figure 8: Curves  $\vec{x}(t)$  fitted with LOWESS for two insect tracks. The fitted curves are coloured and the DVS points are shown in grey.

satisfy:

$$-0.5 \cdot \theta_{t,\text{tolerance}} < t_s - t_e < \theta_{t,\text{tolerance}} \quad (2)$$

This allows for gaps of the length  $\theta_{t,\text{tolerance}}$  and an overlap of half of  $\theta_{t,\text{tolerance}}$ . The gap length has to be greater than the tolerance of overlap because one insect often covers the other. This leads to large gaps in the track. A time overlap that large, however, did not occur in our data, which is why 0.5 was somewhat arbitrarily chosen to reduce the allowed overlap. A threshold that worked in our case was, in the original time unit,  $\theta_{t,\text{tolerance}} = 35\text{ms}$ .

For approximating the outgoing and incoming direction,  $\vec{v}^{in}$  and  $\vec{v}^{out}$  of the tracks, the first PCA component of the beginning and end of every segment is calculated. The size of the beginning and end is determined by a proportion of the size of the segment. The similarity of the directions is measured with the cosine similarity, and a segment  $S_j$  is only considered as a continuation of segment  $S_i$ , if

$$\cos(\vec{v}_j^{in}, \vec{v}_i^{out}) > \theta_{\text{mincos}} = 0.7 \quad (3)$$

Moreover, there is the constraint that each segment cannot be used more than once as a continuation of another segment. If more than one segment fulfils all conditions, the segment with the maximal cosine similarity  $\cos(\vec{v}_j^{in}, \vec{v}_i^{out})$  is chosen as the continuation.

## 2.4 Curve fitting

For visualisation or for an analysis of insect flight patterns, it is useful to represent each track as a spatial curve  $\vec{x}(t)$  that yields a position for every time  $t$ . As each point in our point cloud already has a time stamp, this time coordinate can be used as a predictor in a local regression model with the space coordinates as a multivariate response variable. An established method for local regression is Cleveland's Locally Weighted Estimated Scatterplot Smoothing (LOWESS) (Cleveland, 1979). We used the Open

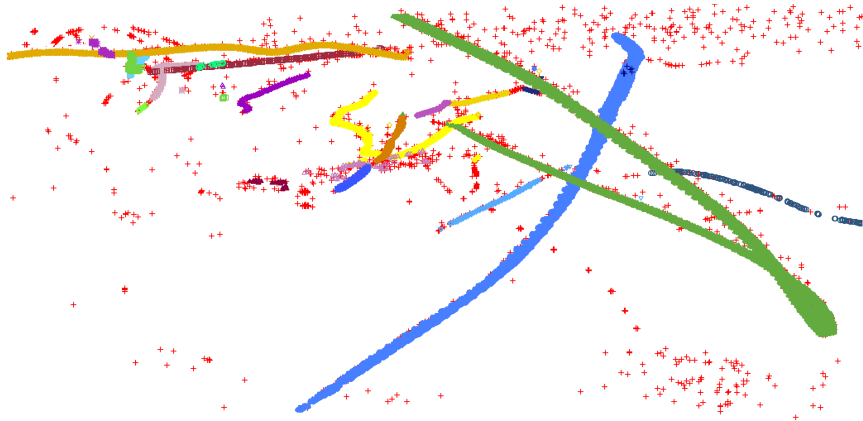


Figure 9: Example result showing the clustering of the points into noise (red) and different insect tracks (other colours).

Source C++ implementation *CppWeightedLowess*<sup>3</sup> by Aaron Lun.

For each time value  $t$ , LOWESS fits a second order polynomial locally through the  $r$  neighbouring points in the predictor space, which is the time in our case. Apart from only using the nearest neighbours, the points are also inversely weighted according to their distance in the predictor space. This restricts the regression further to the local shape. From a set of sample points, LOWESS predicts a response  $\bar{x}(t)$  for arbitrary predictor values  $t$  within the sample range, but the resulting curve is non-parametric. We therefore compute the predicted  $x$  and  $y$  coordinates for equally spaced timestamps and store both together as the result of the curve fitting.

The result of LOWESS depends on the number of neighbours that are used for local fitting, which is determined by a parameter  $f$ , also known as *span*. A smaller value for  $f$  produces a less smooth curve, whereas a larger value result in a smoother curve.  $f$  can be given as a proportion of the entire set, e.g. 10%, or as a fixed number of neighbours. A curve tangential to the flight direction is only obtained, if the neighbourhood extends much more in the flight direction than perpendicular to it. Unfortunately, this means that a fixed number of neighbours does not work for fitting insect tracks in general, because insects vary considerable in size and wing beat rate, which means that the number of DVS events per time interval can vary considerably. Therefore, we chose 0.2 as value for  $f$ , i.e. 20% of the points per cluster were used to fit each value. As can be seen in Figure 8. This may result in overly smoothed curves, however, in cases of very long clusters.

<sup>3</sup><https://github.com/LTLA/CppWeightedLowess>

### 3 RESULTS

We have evaluated our algorithm on eight recordings of insect flights on a meadow that were captured in the context of the BeeVision project (Pohle-Fröhlich and Bolten, 2023). The data was recorded with a Prophesee EVK3 Gen4.1 event camera ( $1280 \times 720$  resolution), where time was recorded in microseconds. The length varied between 16 and 160 seconds, comprising 308MB and about  $10^7$  events. The data points had already been segmented with a U-Net (Pohle-Fröhlich et al., 2024), and the time was scaled to milliseconds.

To obtain ground truth data, the files were manually labelled, assigning each insect track a unique label and an additional label for points considered to be noise. This was done with the Semantic Segmentation Editor<sup>4</sup> that allows for 3D point cloud labelling. To assess the ground truth labelling, a sample of the test data was labelled manually again a few months apart from the first pass. This provided a reference value for the accuracy of the labelling.

To evaluate the post-processing, 19 merges of several tracks into one cluster were identified in the dataset and isolated with some surrounding clusters. To assess the robustness of our algorithm with respect to noise, both the original dataset with noise and the dataset without noise were used.

#### 3.1 Evaluation criteria

There are two categories of evaluation criteria for the evaluation of clusterings, *internal* and *external indices* (Hassan et al., 2024). Internal indices, like the Silhouette Index and Calinski-Harabasz Index, assess clusters based on properties such as intra- and inter-

<sup>4</sup><https://github.com/Hitachi-Automotive-And-Industry-Lab/semantic-segmentation-editor>

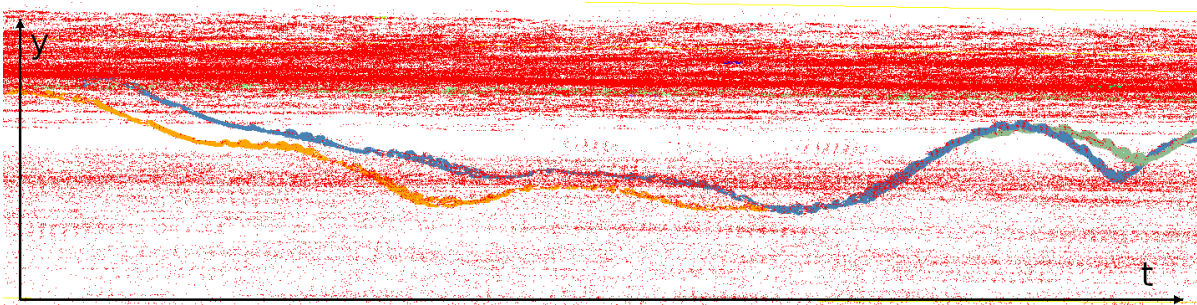


Figure 10: Example for the result of noise removal: red points are noise, the time is on the x-axis and the y-axis is the y-coordinate

cluster variance, but they assume clusters are spherical and are thus not suitable for insect tracks.

External metrics compare the clustering results with ground truth data. These metrics evaluate clusterings by counting whether pairs of points fall in the same or different clusters in the respective clusterings. From these counts, the (adjusted) Rand Index and the Jaccard Score are computed (Hubert and Arabie, 1985). The Rand Index measures overall similarity, ranging from 0 (no matching pairs) to 1 (identical clusterings), while the adjusted Rand Index corrects for chance. The Jaccard Score is similar but only focuses on pairs that are in the same cluster in both ground truth and predicted clustering. This has the effect that the Jaccard Score is always smaller than the Rand Index.

Since these metrics are pair-based, larger clusters (or tracks) with more point pairs will have a greater impact on the evaluation results. Moreover, although their range is  $[0, 1]$ , it is not clear which values actually represent “good” results. We therefore compared the two manual ground truth clusterings of the same data set and obtained a Jaccard-Score of about 0.86 and an adjusted Rand-Score of 0.92. This means that results around these values can be considered as good results for our algorithm.

### 3.2 Clustering

As can be seen from the results in Table 1, in the absence of noise, the MST-based clustering and DBSCAN both have an excellent performance that is comparable to a human. In the presence of noise, however, DBSCAN performs considerably poorer. This is because the MST-based clustering removes more less dense clusters than DBSCAN. An example of its ability to remove noise is seen in Figure 10, where the insect track is mostly separated from the noise with only some small artefacts.

According to Table 1, it seems that the post-processing has almost no effect on the quality of

noise	post-proc.	MST		DBSCAN	
		$R_{adj}$	$J$	$R_{adj}$	$J$
no	no	0.921	0.857	0.919	0.854
no	yes	0.922	0.858	0.922	0.858
yes	no	0.759	0.656	0.598	0.470
yes	yes	0.765	0.662	0.589	0.467

Table 1: Jaccard score  $J$  and adjusted Rand index  $R_{adj}$  for the two clustering algorithms with and without noise or with and without post-processing.

the segmentation. This is misleading, however, because the pairwise quality indices are dominated by the large clusters and not very sensitive to differences in small clusters. Therefore, we did another test with only those clusters that were erroneously merged by the clustering algorithms. Out of 19 merged cluster, the post-processing split 11 correctly, and 3 were correctly split, but not perfectly rejoined. The same test for non-merged clusters yielded no incorrect splits.

Noise removal worked best with uniformly distributed noise but had problems when noise is concentrated in specific areas, e.g., due to ambient effects like wind. For the full original noisy recording with points removed only when are the only point in an octree cube or when they end up in a cluster of only one point, 70.8% of all noise points are correctly removed, while 1.3% of insect points were incorrectly removed. This criterion is thus too strict for raw noisy data. Weaker thresholds are required for noisy datasets, although more aggressive filtering disproportionately affects small insect tracks. More filtering will also remove points at the edges of the insect tracks, which could impact the insect classification downstream. With simulated uniformly distributed noise consisting of about 197% of the original point cloud size, 99.98% of noise points are removed, while only 5.78% of insect points are affected.

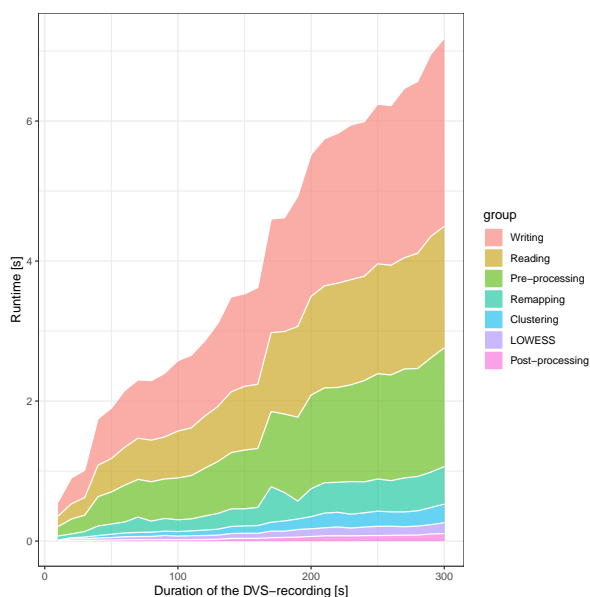


Figure 11: The runtime plotted against the length of the DVS-recording and separated into the individual steps of the processing pipeline.

### 3.3 Runtime

When the method is utilised for actual real-life insect monitoring, it is crucial that the processing occurs in real time, i.e., the runtime must be less than the recording time of the DVS sensor plus other pre-processing time possibly needed, e.g. for computing 3D spatial information from stereo recordings (Pohle-Fröhlich et al., 2024). Figure 11 shows how the average runtime varies with the DVS-recording duration and how it is distributed among the different processing steps. The runtime was measured on an AMD Ryzen 7 5700U CPU running Ubuntu 20.04 and averaged over 100 runs. As can be seen from Figure 11, the processing runtime is always considerably shorter than the duration of the recording.

We also measured the speedup  $S$  due to pre-processing, defined as the runtime without subsampling divided by the runtime with subsampling. The speedup for noise filtering was greater in unnoisy data ( $S \approx 20$ ) than in noisy data ( $S \approx 4$ ). This is because subsampling reduces the number of noisy points less effectively, as many noise points occupy their own cubes. The speedup for noisy data increases with noise removal during subsampling. This in particular affected the MST-based clustering which had a speedup of 30. This means that subsampling is essential for an application in real time.

## 4 CONCLUSIONS

We have developed a method for fast instance segmentation of insect flight tracks in DVS data, treating time as another dimension to preserve high temporal resolution. The central part of the algorithm is a density based clustering, for which either DBSCAN or MST-based clustering can be chosen. The MST-based clustering was considerably more robust with respect to noise and is thus preferable. Both algorithms, however, failed to separate close by tracks, and we have implemented a post-processing step that remedies this shortcoming in most situations.

Due to subsampling during pre-processing, the method has a runtime much shorter than the DVS recording duration and is thus applicable in real time. Noise removal was optionally included in the subsampling step and in the clustering step. These automatic noise detection makes the method quite robust in the presence of noise, which is important for its deployment in natural scenarios.

Although the method has an accuracy comparable to a manual segmentation by a human, it occasionally removes thin tracks. This makes the method currently less effective for small insects like mosquitos. For visualisation or further analysis, we also fit flight trajectories through the returned clusters. Although our usage of LOWESS was satisfactory, a local regression based on the number of neighbours can become problematic for scenarios with a wide range of track thicknesses and lengths. It would be interesting to investigate different local regression methods, e.g. by basing the local region on fixed time intervals.

Although we tested our method only with DVS data with two spatial dimensions, there is nothing special in our algorithm that restricts it to 2D data. The method can thus readily be deployed to 3D data like that recorded by the new system developed in the Bee-Vision project (Pohle-Fröhlich et al., 2024), which aims at counting insect populations over a long period. We plan to deploy our algorithm in this project and use it as a second step after semantic segmentation. This will then be followed by a classification step which leads to an automatic counting of species occurrences in the data.

## REFERENCES

- Cleveland, W. S. (1979). Robust locally weighted regression and smoothing scatterplots. *Journal of the American Statistical Association*, 74(368):829–836.
- Dalitz, C., Ayyad, Y., Wilberg, J., Aymans, L., Bazin, D., and Mittig, W. (2019a). Automatic trajectory recognition in Active Target Time Projection Chambers



- data by means of hierarchical clustering. *Computer Physics Communications*, 235:159–168.
- Dalitz, C., Wilberg, J., and Aymans, L. (2019b). TriplClust: An algorithm for curve detection in 3D point clouds. *Image Processing On Line*, 8:26–46.
- Ester, M., Kriegel, H.-P., Sander, J., Xu, X., et al. (1996). A density-based algorithm for discovering clusters in large spatial databases with noise. In *kdd*, volume 96, pages 226–231.
- Hallmann, C. A., Sorg, M., Jongejans, E., Siepel, H., Hofland, N., Schwan, H., Stenmans, W., Müller, A., Sumser, H., Hörren, T., et al. (2017). More than 75 percent decline over 27 years in total flying insect biomass in protected areas. *PLoS one*, 12(10):e0185809.
- Hassan, B. A., Tayfor, N. B., Hassan, A. A., Ahmed, A. M., Rashid, T. A., and Abdalla, N. N. (2024). From A-to-Z review of clustering validation indices. *Neurocomputing*, 601:128198.
- Hubert, L. and Arabie, P. (1985). Comparing partitions. *Journal of classification*, 2:193–218.
- March, W. B., Ram, P., and Gray, A. G. (2010). Fast Euclidean minimum spanning tree: algorithm, analysis, and applications. In *Proceedings of the 16th ACM SIGKDD international conference on Knowledge discovery and data mining*, pages 603–612.
- Meagher, D. (1982). Geometric modeling using octree encoding. *Computer graphics and image processing*, 19(2):129–147.
- Pohle-Fröhlich, R. and Bolten, T. (2023). Concept study for dynamic vision sensor based insect monitoring. In *International Conference for Computer Vision and Applications (VISAPP)*, pages 411–418.
- Pohle-Fröhlich, R., Gebler, C., and Bolten, T. (2024). Stereo-event-camera-technique for insect monitoring. In *International Conference for Computer Vision and Applications (VISAPP)*, pages 375–384.
- Rovere, M., Chen, Z., Di Pilato, A., Pantaleo, F., and Seez, C. (2020). CLUE: A fast parallel clustering algorithm for high granularity calorimeters in high-energy physics. *Frontiers in Big Data*, 3:591315.
- Schubert, E., Sander, J., Ester, M., Kriegel, H. P., and Xu, X. (2017). DBSCAN revisited, revisited: why and how you should (still) use DBSCAN. *ACM Transactions on Database Systems (TODS)*, 42(3):1–21.
- Zahn, C. T. (1971). Graph-theoretical methods for detecting and describing gestalt clusters. *IEEE Transactions on Computers*, 100(1):68–86.